Narrow width Farley-Buneman spectra under strong electric field conditions

Jean-Pierre St.- Maurice[1], Devin Huyghebaert[2], Magnus Fagernes Ivarsen[3], and Glenn C. Hussey[3]

[1]U of Saskatchewan
[2]UiT The Arctic University of Norway
[3]University of Saskatchewan

December 7, 2022

Abstract

As a rule, the phase velocity of unstable Farley-Buneman waves is found not to exceed the ion-acoustic speed, cs. However, there are known exceptions: under strong electric field conditions, much faster Doppler shifts than expected c_s values are sometimes observed with coherent radars at high latitudes. These Doppler shifts are associated with narrow spectral width situations. To find out how much faster than c_s these Doppler shifts might be, we developed a proper c_s model as a function of altitude and electric field strength based on ion frictional heating and on a recently developed empirical model of the electron temperature under strong electric field conditions. Motivated by the 'narrow fast' observations, we then explored how ion drifts in the upper part of the unstable region could add to the Doppler shift observed with coherent radars. While there can be no ion drift contribution for the most unstable modes, and therefore no difference with c_s for such modes, under strong electric field conditions, a large ion drift contribution of either sign needs to be added to the Doppler shift of more weakly unstable modes, turning them into 'fast-' or 'slow-' narrow spectra. Particularly between 110 and 115 km, the ion drift can alter the Doppler shift of the more weakly unstable modes by several 100 m/s, to the point that their largest phase velocities could approach the ambient E x B drift itself.

Narrow width Farley-Buneman spectra under strong electric field conditions

Jean-Pierre St-Maurice[13], Devin Huyghebaert[4], Magnus F. Ivarsen[12], and Glenn C. Hussey[1]

[1]Department of Physics and Engineering Physics, University of Saskatchewan, Saskatoon, Saskatchewan, Canada
[2]Department of Physics, University of Oslo, Oslo, Norway
[3]Department of Physics and Astronomy, University of Western Ontario, London, Ontario, Canada
[4]Department of Physics and Technology, UiT The Arctic University of Norway, Tromsø, Norway

Key Points:

- The ion drift under strong electric field conditions has a strong impact on the Doppler shift of weakly unstable modes
- Non-isothermal ions must be included in the calculation of Doppler shifts above 110 km, particularly for the more weakly growing modes
- The largest Doppler shifts that can be observed in Farley-Buneman waves is from narrow spectra near 114 km when the E field exceeds 50 mV/m

Abstract

As a rule, the phase velocity of unstable Farley-Buneman waves is found not to exceed the ion-acoustic speed, c_s. However, there are known exceptions: under strong electric field conditions, much faster Doppler shifts than expected c_s values are sometimes observed with coherent radars at high latitudes. These Doppler shifts are associated with narrow spectral width situations. To find out how much faster than c_s these Doppler shifts might be, we developed a proper c_s model as a function of altitude and electric field strength based on ion frictional heating and on a recently developed empirical model of the electron temperature under strong electric field conditions. Motivated by the 'narrow fast' observations, we then explored how ion drifts in the upper part of the unstable region could add to the Doppler shift observed with coherent radars. While there can be no ion drift contribution for the most unstable modes, and therefore no difference with c_s for such modes, under strong electric field conditions, a large ion drift contribution of either sign needs to be added to the Doppler shift of more weakly unstable modes, turning them into 'fast-' or 'slow-' narrow spectra. Particularly between 110 and 115 km, the ion drift can alter the Doppler shift of the more weakly unstable modes by several 100 m/s, to the point that their largest phase velocities could approach the ambient $\mathbf{E}\times\mathbf{B}$ drift itself.

Plain Language Summary

HF and UHF radars routinely detect the presence of turbulence in the aurora between 100 and 120 km altitudes. The turbulent structures are excited whenever the electric field produces much larger electron than ion drifts. At their largest amplitudes, the structures end up moving at the ion acoustic speed, which can be much less than the electron drift at times. The ion-acoustic speed comes from large amplitude structures reducing the driving electric field until they can no longer grow. The present paper deals with the fact that the ion-acoustic speed motion is actually in the ion frame of reference. For strong electric field situations, the ion motion in the upper part of the unstable region is large enough to make the Doppler shifts observed from the ground either markedly faster or markedly slower than the ion-acoustic speed, c_s. However, we also show that this deviation from c_s is largest for weakly-unstable/ weakly-turbulent modes in which the observed spectra exhibit particularly narrow spectral widths. We also find that there is a real, but smaller, reduction from c_s for weakly turbulent spectra in the lower part of the instability region, near 104 km altitude.

1 Introduction

When looking perpendicular to the magnetic field lines, radars frequently observe echoes associated with plasma irregularities. The E region below 130 km altitude is a particularly rich source of echoes at high latitudes under disturbed magnetic conditions. For 10 MHz and higher radar frequencies, it is now well established that when the ambient electric field is such that the magnitude of the $\mathbf{E}\times\mathbf{B}$ drift, E/B, exceeds about 400 m/s, radar echoes from large amplitude plasma structures are detected. The origin of the structures is known to be the Farley-Buneman (FB) plasma instability, which is produced by Hall currents whenever the relative drift between ions and electrons is larger than the ion-acoustic speed. The large Hall currents are produced because, below 120 km, the ions become weakly magnetized while, in the same region, the electrons are strongly magnetized. Several comprehensive reviews exist on the nature and origin of the instability (e.g., Fejer & Kelley, 1980; Hysell, 2015; Kelley, 1989), and need not be repeated here.

Interesting examples of Doppler shifts that are much faster than the expected c_s value have been found at high latitudes over the years and many, if not all, of these examples are associated with narrow width spectra (e.g, Chau & St-Maurice, 2016; Sahr

& Fejer, 1996). It has been suggested by St-Maurice and Chau (2016) that the unusual Doppler shifts came from the addition of an ion drift contribution to the (already enhanced) c_s speed, given that the waves are produced in the ion frame of reference. We pursue this line of thought in the present paper with an important modification due to the fact that the ion drift is always perpendicular to the relative electron-ion drift, $\mathbf{v}_d$. We show that this means that the Doppler shift of the fastest growing, most unstable modes, is not affected by the ion drift. However, as the line-of-sight moves away from the most unstable direction, the ion drift is able to introduce a strong contribution, particularly in the upper portions of the unstable E region. The fastest Doppler shifts would end up being found for the largest angular deviations from the $\mathbf{v}_d$ direction and be associated with particularly narrow spectral widths (so-called Type IV waves in the literature). The goal of the present paper is to assess in precise terms what the maximum Doppler shift values should actually be, and then to compare the theory with available information from observations. We note that the theory also predicts the occurrence of narrow spectra with Doppler shifts substantially less than c_s (so-called Type III, in the literature). The theory behind this related effect is included here. A comparison with observations of slow and fast spectra with narrow spectral widths is also carried out in the present work.

In Section 2 we quickly address important relevant properties of interest regarding the background plasma. We first discuss the relative drift between ions and electrons. Next, we introduce a model of the isothermal ion-acoustic speed. Both properties need to be clearly documented as a function of altitude and electric field strength for what follows. Section 3 explores the properties of the unstable structures with an emphasis on the high altitude portion of the unstable region. Section 4 discusses how the phase velocities should go through a maximum somewhere above 110 km as a result of a combination of nonlinear wave properties and of non-negligible contributions from the ion motion. Three different models are constructed, compared and discussed. The models even open up the possibility to extract useful electric field information particularly in the presence of fast Doppler shifts in the higher parts of the unstable region. The connection with slow narrow spectra from the upper E region is also presented in that section. Section 5 provides examples from recent observations from VHF radars. This includes the newly built ICEBEAR 3D radar with its capability to accurately localize the altitude of echoes.

2 Background properties of interest

2.1 Drift considerations

In the presence of an electric field $\mathbf{E}$ perpendicular to the geomagnetic field, the ion drift as a function of altitude is given by a well-known solution to the steady state ion momentum equation. After neglecting neutral wind effects and taking away the small pressure gradient contributions, the solution takes the form (e.g., St-Maurice et al., 1999)

$$\mathbf{v}_i = \frac{\mathbf{E}}{B}\frac{\alpha_i}{1+\alpha_i^2} + \frac{\mathbf{E}\times\mathbf{b}}{B}\frac{1}{1+\alpha_i^2} \tag{1}$$

where $\alpha_i = \nu_i/\Omega_i$ with the symbols ν and Ω denoting the collision frequency with neutrals and the cyclotron frequency, and the subscript i standing for 'ions'.

As discussed in more detail below, it is important to know the relative drift between ions and electrons in strong electric field situations, since the unstable waves are produced in the ion frame of reference (e.g., Fejer & Kelley, 1980). Above 100 km (the region of insterest in the present work), the electrons can be assumed to be $\mathbf{E}\times\mathbf{B}$ drifting to a high degree of accuracy, since $\nu_e << \Omega_e$. This means that relative drift, $\mathbf{v}_d$, between ions and electrons is given quite accurately by

$$\mathbf{v}_d \equiv \mathbf{v}_e - \mathbf{v}_i = \frac{\mathbf{E}\times\mathbf{b}}{B}\frac{\alpha_i^2}{1+\alpha_i^2} - \frac{\mathbf{E}}{B}\frac{\alpha_i}{1+\alpha_i^2} \tag{2}$$

A property that proves to be quite important is that the ion drift $\mathbf{v}_i$ is perpendicular to the relative drift $\mathbf{v}_d$. This can easily be shown from Equations (1) and (2) since the dot product $\mathbf{v}_i \cdot (\mathbf{v}_e - \mathbf{v}_i) = 0$.

We will also require later on to deal with the magnitudes of $\mathbf{v_d}$ and $\mathbf{v}_i$. From the above expressions it is easy to show that they are given by

$$v_d = \frac{E}{B}\frac{\alpha_i}{\sqrt{1+\alpha_i^2}} \tag{3}$$

$$v_i = \frac{E}{B}\frac{1}{\sqrt{1+\alpha_i^2}} \tag{4}$$

so that $v_i/v_d = 1/\alpha_i$. In the model used in this paper, the ratio is less than 1 below 118 km, where α_i passes through the value of 1. This means that, since the ion collision frequency decreases exponentially with altitude, the relative drift in the ion frame of reference decreases rapidly past the $\alpha_i = 1$ altitude (118 km in our model calculations).

2.2 The isothermal ion-acoustic speed

The isothermal ion-acoustic speed, c_s, is a critical parameter to ascertain in the FB instability problem because v_d has to exceed c_s for the plasma waves to grow at all. Some non-isothermal corrections exist under certain conditions to be discussed below, but c_s remains a key reference. While c_s is relatively constant in the presence of weaker electric fields, the situation is very different with very strong electric fields, just when the FB instability is strongly excited. It therefore proves important to see how c_s varies in the unstable region when strong electric fields are present.

The isothermal ion-acoustic speed is given by the well-known expression

$$c_s = \sqrt{k_b(T_i + T_e)/m_i} \tag{5}$$

where k_b is the Boltzman constant, m_i is the ion mass and T_e and T_i are the electron and ion temperatures, respectively. A proper calculation of c_s therefore requires a good handle of the ion and electron temperatures as functions of altitude during strong electric field events.

For T_i, we use well-known ion frictional heating expressions (e.g., St-Maurice & Chau, 2016)

$$T_i = T_n + \frac{m_n}{3k_b}v_i^2 = T_n + \frac{m_n}{3k_b}\frac{(E/B)^2}{1+\alpha_i^2} \tag{6}$$

where m_n is the mean mass of neutral constituents. Here we again neglect the neutral drift $\mathbf{v}_n$, which can sometimes have non-negligible effects but cannot be determined from coherent radar observations alone. Neglecting the effect of $\mathbf{v}_n$ amounts to stating that our discussion pertains not so much to the electric field but rather to the effective electric field $\mathbf{E}' = \mathbf{E}+\mathbf{v}_n\times\mathbf{B}$ (St-Maurice et al., 1999). In the end, the key element needed for the calculation of T_i is α_i, which requires the ion-neutral collision frequency. We used the collision frequencies posted in Schunk and Nagy (2009) together with MSIS model for the neutral densities, after scaling it in such a way as to have α_i equal to 1 at 118 km altitude, following the work of Sangalli et al. (2009).

This brings us to a calculation of T_e. There is now, fortunately, a simple way to handle T_e based on an empirical model that has been developed by St-Maurice and Goodwin (2021). The model used exceptionally good incoherent radar data from a very strong

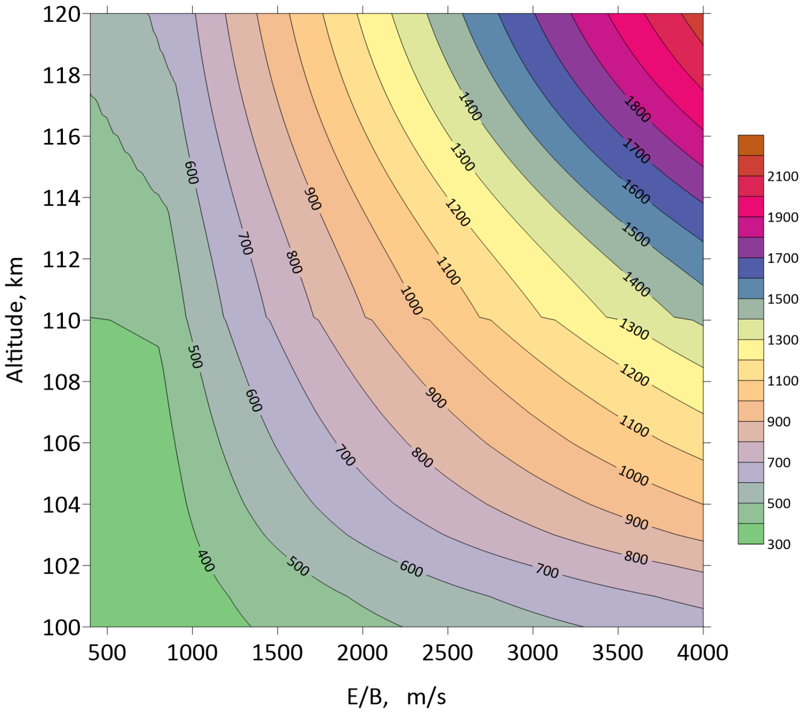

Figure 1. Modeled isothermal ion-acoustic speed in m/s, as a function of E/B and altitude

electric field event observed by RISR-N. It established/confirmed that T_e responds to E/B essentially in linear fashion once the E/B exceeds 800 m/s. St-Maurice and Goodwin (2021) found that this unexpectedly simple feature means that the heating rate produced by unstable plasma wave is basically associated with E/B to the power 3 or 4, depending on the electric field strength.

Thus, in the present work, we have used the St-Maurice and Goodwin (2021) values and expressions. For E/B in excess of 800 m/s, this meant having

$$T_e = T_{e0} + C_e(E/B - 800) \tag{7}$$

where T_{e0} and C_e were tabulated as functions of altitude by St-Maurice and Goodwin (2021). Note that T_{e0} is based on an estimate for the neutral temperature, T_n, and that for $E/B < 800$ m/s we simply used $T_e = T_n$.

Figure 1 shows the resulting calculated variations in the ion-acoustic speed as a function of E/B and altitude based on expressions (5), (6) and (7). For $E/B < 800$ m/s, T_i, like T_e, is for the most part quite close to T_n since ion frictional heating is not large in that case at the altitudes of interest. This explains why Figure 1 shows only a modest increase in c_s with altitude if $E/B < 1000$ m/s. The small increase is largely the result of a modest increase in T_n with altitude. This means that typical c_s values are between 350 and 600 m/s for $E/B < 1000$ m/s. By contrast, it can also be seen from the same Figure 1 that the ion acoustic speed should be greater than 1300 m/s above 110 km with electric fields of 150 mV/m (E/B = 3000 m/s). Already, values in excess of 1000 m/s are found above 110 km altitude if E/B exceeds 2000 m/s. This stated, for altitudes less than 110 km, c_s remains less than 800 m/s even for $E/B \approx 2000$ m/s.

3 Phase velocities of FB waves at the top of the unstable layer

According to linear FB instability theory, we must have (e.g., Fejer et al., 1975)

$$\omega_r = \frac{\mathbf{k} \cdot (\mathbf{v}_e + \Psi \mathbf{v}_i)}{1+\Psi} = \frac{\mathbf{k} \cdot (\mathbf{v}_e - \mathbf{v}_i)}{1+\Psi} + \mathbf{k} \cdot \mathbf{v}_i \tag{8}$$

Here, ω_r is the real part of the frequency, and $\mathbf{k}$ is the wavevector for a particular unstable direction. If the aspect angle can be neglected, (near-perpendicularity of $\mathbf{k}$ to the magnetic field), $\Psi = \nu_e \nu_i/(\Omega_e \Omega_i)$. Importantly for what follows below, this expression for the frequency clearly states that the unstable waves are produced in the ion frame of reference.

The growth rate, γ, from the linear FB instability theory is given by (e.g., Fejer et al., 1975)

$$\gamma = \frac{\Psi/\nu_i}{1+\Psi} \left[(\omega_r - \mathbf{k} \cdot \mathbf{v}_i)^2 - k^2 c_s^2 \right] \tag{9}$$

It follows from equations 8 and 9 that the most unstable modes (fastest growing) are found when $\mathbf{k}$ points in the $\mathbf{v}_d$ direction. We also note that if the plasma waves move at close to the threshold speed (near zero growth rate condition) we should have

$$(\omega_r - \mathbf{k} \cdot \mathbf{v}_i)^2 = k^2 c_s^2 \tag{10}$$

We have already seen that c_s increases with altitude while v_d decreases with altitude. This means that when v_d is large enough to have instability somewhere in the E region, there has to be an upper altitude cutoff at which the growth rate becomes very small. This upper altitude cutoff is determined from the altitude at which v_d has gone down to become equal to c_s. This condition applies to all destabilizing electric field conditions, be they weakly or strongly destabilizing.

Thus, at the upper altitude boundary of the instability, we would have $\omega_r = (kc_s + \mathbf{k} \cdot \mathbf{v}_i)$. However the only waves that would grow there would have to be in the $\mathbf{v}_d$ direction, which, as seen in the previous section, happens to be always perpendicular to $\mathbf{v}_i$. Using the fact that $\omega_r \to \mathbf{k} \cdot \mathbf{v}_d$ and that the only unstable modes are for $\mathbf{k}$ parallel to $\mathbf{v}_d$ the phase velocity, v_{ph}, at the upper portion of the unstable layer would have to be given by the condition $v_{ph} = v_d = c_s$ with the waves pointing in the $\mathbf{v}_d$ direction. Below that upper altitude cutoff, $\mathbf{v}_{ph}$ need not point in the $\mathbf{v}_d$ direction. This means, as we discuss next, that the ion drift will affect the Doppler shift in the upper portions of the unstable region, though not near the upper boundary itself.

4 The fastest phase velocities in strongly-driven cases and how these relate to the $\mathbf{E} \times \mathbf{B}$ drift.

As seen/discussed in section 2, the c_s profile is very different in the presence of a strong electric field. The ion drift then also becomes significant higher up and the altitude at which v_d exceeds c_s could even go above 120 km. This means that a potentially large ion drift contribution would now need to be taken into account.

As eluded to above, the ion drift does not contribute to the Doppler shift of the fastest growing modes, which are along $\mathbf{v}_d$. However, if the angular width of the 'instability cone' is β_M and if we can assume, for example, that all unstable waves within that cone move at c_s in the ion frame of reference (more on this below), then a Doppler shift as large as $c_s + v_i \sin \beta_M$ could be observed. Being on the edge of the instability cone, such waves, like those at the top of the unstable region, would have narrow spectral widths, owing to their weak growth rate, i.e., weakly turbulent state.

We illustrate the two Doppler shift possibilities in Figure 2. The cartoon from that figure illustrates that if a radar line-of-sight points between the $\mathbf{v}_d$ and $\mathbf{v}_i$ directions as

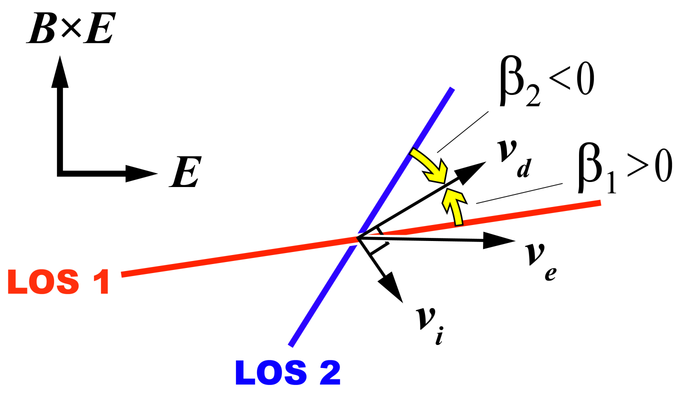

Figure 2. Cartoon illustrating how the ion drift contributes to the Doppler shift of waves growing outside the direction indicated by $\mathbf{v}_d$. If the line-of-sight is along the red line ('los 1'), i.e. between $\mathbf{v}_d$ and $\mathbf{v}_i$, the ion drift and $\mathbf{v}_d$ components add up along the line-of-sight ($\beta > 0$ case). For all other directions, such as with the 'los 2' blue line ($\beta < 0$ case), they work in opposite direction.

shown for 'Los 1', the components of a phase velocity in the $\mathbf{v}_d$ direction projected along the line of sight will be added to the component of $\mathbf{v}_i$ along the line-of-sight. For all other directions of the line-of-sight, like 'Los 2', the components work in opposite directions and the total Doppler shift is diminished.

At this point, the results depend on additional details about the nonlinear evolution of the unstable waves, which determine the nonlinear phase velocities as a function of direction. Under the assumption of isothermal conditions there are two contrasting positions. The first one, which we will call here the 'St-Maurice and Hamza' condition, is one for which the phase velocity of the largest amplitude modes is equal to c_s in the ion frame of reference for all unstable directions, i.e. everywhere inside the instability cone. An alternative has been proposed by Hysell and co-workers and will be labeled here as the 'Hysell' condition. In addition, Dimant and Oppenheim (2004) have pointed out that the instability may not be treated through isothermal ions in the upper part of the unstable region. The non-isothermal ion consequences for the Doppler shift in situations where the ion drift matters will therefore also be presented.

4.1 The case for saturation of unstable modes at a phase speed c_s in the ion frame

4.1.1 Saturation at c_s in the ion frame of reference

Numerous radar observations from the lower part of the unstable region (e.g., Hysell, 2015, and references therein), numerical simulations (e.g, Oppenheim & Dimant, 2013, and references therein), and theoretical considerations (e.g., St-Maurice & Hamza, 2001) have led researchers to conclude that, in the region where there is no need to consider the impact of the ion drift on the Doppler shift, the maximum Doppler shift of observed radar spectra does not exceed c_s, or more generally speaking, the instability threshold speed. This Doppler shift is observed in directions for which the plasma is expected to be unstable. The Doppler shift is smaller than c_s for spectra observed in directions for which the linear theory predicts stability, implying that in those directions, mode-coupling is at work. The spectra with Doppler shift of the order of c_s have been dubbed as 'Type I' and the slower types, which have typically larger spectral widths, have been dubbed as 'Type II'. In what follows we assume that the situation is the same higher up where the ion drift matters, with the caveat that we should allow for the fact that the c_s saturation takes place in the ion frame of reference which is itself moving with respect to the ground.

4.1.2 Predictions based on the nonlinear 'St-Maurice and Hamza' model

It is important to realize that (1) radar observations are biased to the largest amplitude structures, $\delta n_{\mathbf{k}}$, of the turbulent plasma because the cross section is proportional to $|\delta n_{\mathbf{k}}|^2$ (e.g., St. Maurice & Schlegel, 1983) and (2) that if the largest amplitude structures move at the ion-acoustic speed it can only be because their electric field, $\mathbf{E}^{in} = (\mathbf{E}_0 + \delta\mathbf{E}_{\mathbf{k}})$ is lower than ambient and such that the component of the $\mathbf{E}^{in} \times \mathbf{B}$ drift that is perpendicular to the long axis of the structures is equal to the threshold speed, namely, c_s (here, $\mathbf{E}_0$ stands for the ambient electric field and $\delta\mathbf{E}_k$ stands from the electric field produced by the density perturbations associated with the large amplitude structures, or 'waves'). This actually means that the instability does what it is supposed to do, i.e., bring the plasma to stability, but with the caveat that this can only happen inside individual structures, and not everywhere at once.

The reason for the incomplete coverage of the plasma by depleted electric fields (intermittency) in the unstable regions is that the structures have to decay after having reached a maximum amplitude, owing to the fact that non-local effects necessarily trigger the growth, along the magnetic field, of perturbed electric fields. This forces the structures to dissipate through a shorting of their electric field (Drexler et al., 2002). The notion of an electric field that decays inside unstable structures after having reached a maximum amplitude is supported by high resolution interferometric CW radar observations carried out by Prikryl et al. (1988, 1990) who found clear examples of unstable (growing) plasma waves that moved at much faster velocities than the ion acoustic speed at first -when their amplitude was small- only to slow down to a 'heated' ion-acoustic speed type of phase velocity when the waves reached their maximum amplitude, after which they quickly dissipated.

4.1.3 Electric field reduction inside unstable FB structures

Sato (1973) and, later on, St-Maurice and Hamza (2001) described how electric fields inside large amplitude structures would become weaker in response to growing density fluctuations. Sato (1973) used a mode-coupling approach in which a large primary wave vector $\mathbf{k}_p$ was pointing in the original (most unstable) plane wave direction, namely, the $\mathbf{E}\times\mathbf{B}$ direction. A much smaller $\mathbf{k}_s$ was then added along the background electric field direction, i.e. along what had been the trough or crest lines of the original plane wave. In that context, the $\mathbf{k}_s$ direction was following the long axis of a structure that was perpendicular to the $\mathbf{k}_p$ direction. The original structure could therefore no longer be described in terms of a superposition of pure plane waves in the $\mathbf{E} \times \mathbf{B}$ direction.

St-Maurice and Hamza (2001) followed a different route but ended up with the exact same results. The mode-coupling issue was only implicit in their work. The model simply considered how the electric field inside elongated structures had to rotate and decrease, owing to secondary but important electron Hall drifts in the $\mathbf{k}_s$ direction, which for the most unstable modes would have been the original electric field direction since ion mean drifts were neglected. These Hall drifts generated electric fields along the long axis of the structures in much the same way as the linear instability did in the original $\mathbf{k}_p$ direction, namely, with density gradients along the $\mathbf{k}_s$ direction, the electrons Hall currents had to be balanced by the ion Pedersen currents, thereby creating a polarization electric field that could be computed.

As mentioned, in spite of their different takes on the problem, Sato (1973) and St-Maurice and Hamza (2001) ended up with the same expression for the electric fields inside unstable structures, using current continuity arguments across the structures in both the $\mathbf{k}_p$ and $\mathbf{k}_s$ directions. The result for the electric field inside the structures, $\mathbf{E}^{in}$, was given by

$$\mathbf{E}^{in} = \frac{\mathbf{E}_0 + X\mathbf{E}_0 \times \mathbf{b}}{1 + X^2} \tag{11}$$

where $\mathbf{E}_0$ is the background (or ambient) electric field, $\mathbf{b}$ is a unit vector in the magnetic field direction, $X = \alpha\delta n/n_0$ and $\alpha = \alpha_i/(1+\Psi)$. The parameter α is the negative of the ratio of the Hall to Pedersen conductivities, $-\sigma_H/\sigma_P$, and is readily extracted from equation 2. Note that $X > 0$ for density enhancements (or 'blobs') and $X < 0$ for density depletions (or 'holes'). In view of the above discussion we could also use the notation δn_{k_p} instead of δn to signify that the expression relates to fluctuations associated with instability in the original $\mathbf{k}_p$, or primary wave vector, direction. We note that when $X << 1$ the electric field inside is not too different from the ambient field and that the small electric field correction produces a well-known expression extracted from linear instability theory, namely, $\delta\mathbf{E}_{k_p} \to X\mathbf{E}_0 \times \mathbf{b}$.

From equation (11) it is easy to see that the electric field inside rotates toward the $\mathbf{E}_0 \times \mathbf{B}$ directions and that its magnitude becomes smaller according to

$$|\mathbf{E}^{in}| = \frac{E_0}{\sqrt{1+X^2}} \tag{12}$$

The $1/(1+X^2)$ dependence ensures that as the amplitude grows, the nonlinear phase velocity slows down.

Consider next a situation for which $\mathbf{k}_p$ is not parallel to $\mathbf{v}_d$. Since elongated structures are an essential construct of the FB instability theory, most of the diffusion that slows down the growth has to be in the $\mathbf{k}_p$ direction, i.e. diffusion occurs perpendicularly to the direction of elongation (which started as 'wave fronts' at the linear stage). It has to follow that threshold conditions are met without significant changes in the electric field of the structures whenever $\mathbf{k}_p \cdot \mathbf{v}_d^{in} = k_p v_d^{in} \cos\beta_M = k_p c_s(1+\Psi) = k_p c_s^*$. In these expressions, the use of c_s^* instead of c_s is just to shorten the notation. Also β_M is the largest $\mathbf{k_p}$ angle with respect to $\mathbf{v}_d$ at which structures can grow. We re-emphasize that for such structures $X << 1$ so that $\mathbf{E}^{in} \approx \mathbf{E}_0$, i.e., v_d^{in} is actually simply given by equation 3 when we are interested in the largest angles at which waves can grow.

4.1.4 Fastest Doppler shifts predicted by the nonlinear St-Maurice and Hamza model

As already stated above, since $\mathbf{v}_i \perp \mathbf{v}_d$, the ion drift contribution to the Doppler shift is non-existent for the fastest growing modes. For other modes, if the wave vector is at an angle β to the $\mathbf{v}_d$ direction, an ion drift contribution equal to $v_i \sin\beta$ needs to be added. In the St-Maurice and Hamza model, the velocity along any value of $\mathbf{k}_p$ for which there is growth becomes equal to c_s^* in the ion reference frame. This means that the Doppler shifts that can be observed are on the edges of the unstable cone and that, if the ions can be assumed to be isothermal, they are given by

$$v_{ph}^{max} = c_s^* \pm v_i\sqrt{1 - \frac{c_s^{*2}}{v_d^2}} = c_s^*\left[1 \pm \sqrt{\left(\frac{E}{B}\frac{1}{c_s^*}\right)^2 \frac{1}{1+\alpha_i^2} - \frac{1}{\alpha_i^2}}\right] \tag{13}$$

Being interested at this point in the fastest possible Doppler shifts that can be observed, we focus our study on the root with the + sign for the time being. The other thing to note is that the argument inside the square root operator must be greater or equal to zero. If it is equal to zero, the waves are located at the top of the unstable layer and there

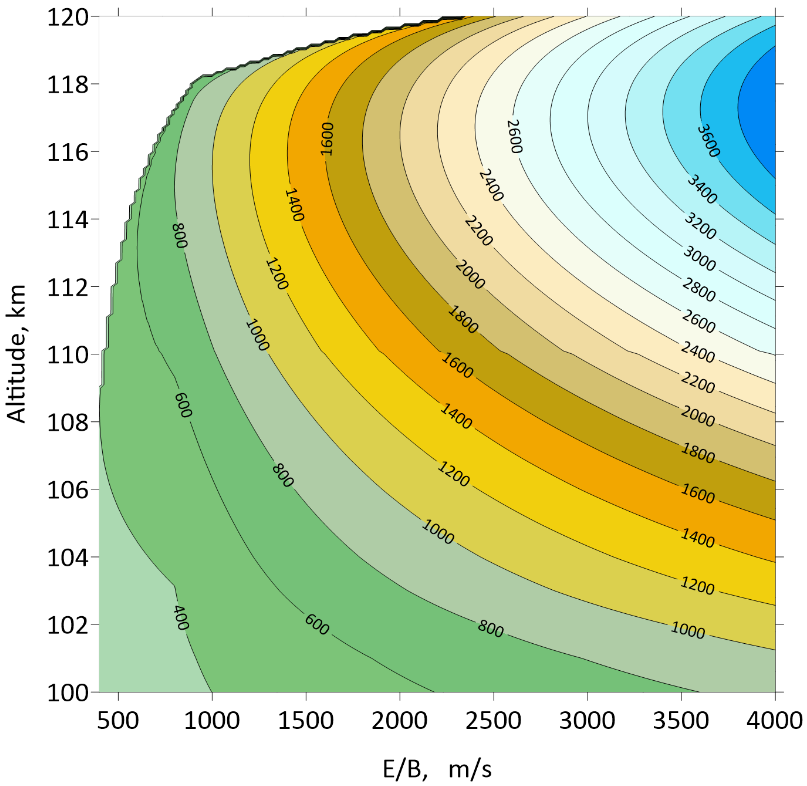

Figure 3. Contours of maximum phase velocities that can be observed by a ground-based observer when ion drift contributions are included, the instability is isothermal, and with c_s saturation along any and all unstable $\mathbf{k}_p$ directions.

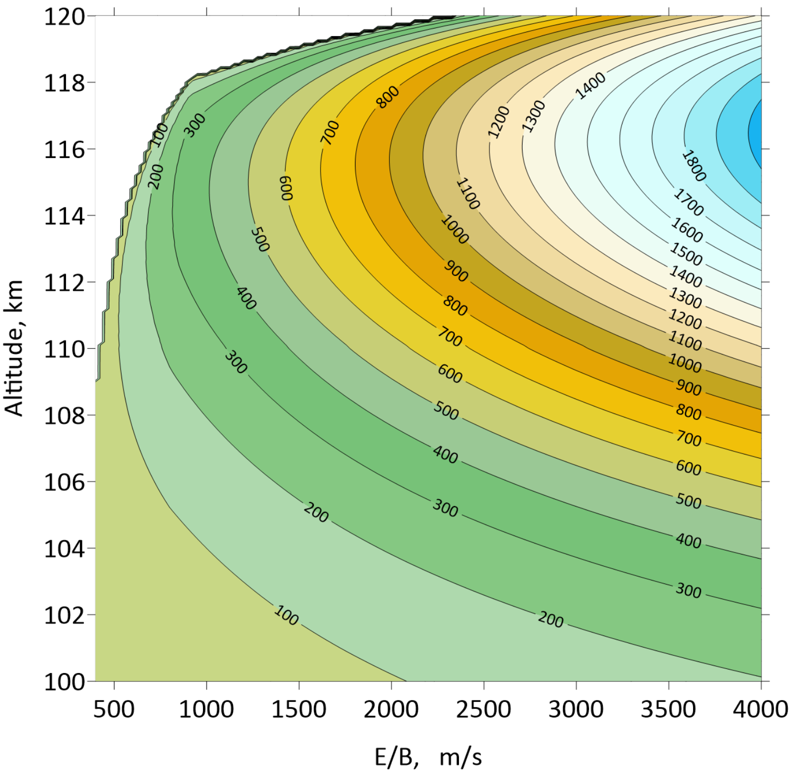

Figure 4. Contours of the difference between the maximum phase velocities shown in Figure 3 and the ion-acoustic speed shown in Figure 1.

is, once again, no ion drift contribution, as discussed in Section 3. In that case, as stated there, $v_{ph} = v_d = c_s^*$.

Figure 3 shows the fastest phase velocities that can be observed under the conditions just described, namely: saturation of all phase velocities in unstable directions at c_s^* relative to the ion drift direction, with the ion drift component along the line-of-sight being added, as indicated by Figure 2. We have chosen to stop the calculations for $E/B =$ 4000 m/s (roughly a 200 mV/m electric field). While stronger electric fields are known to exist, fields in excess of 150 mV/m are rarely detected by radars. Figure 3 makes all the relevant points. First it shows that, if the isothermal assumption holds, the maximum observable phase velocity can become rather close to the value of E/B at altitudes between 112 and 118 km. The position of that peak moves up as the electric field strength increases because the ion-acoustic speed stops increasing with altitude at some point (the T_e increases are more moderate), so that if the relative drift between electrons and ions is still large enough to have instability, the instability cone widens and the ion drift contribution along the line of sight increases. It should be repeated here that when the Doppler shift is very close to E/B in narrow fast spectra, the line-of-sight must be close to the $\mathbf{E}\times\mathbf{B}$ direction, since the unstable waves cannot be moving faster than the electrons.

The point about the ion drift contribution being considerable higher up is perhaps made clearer with the help of Figure 4 which shows the difference between the largest drift of Figure 3 and the ion-acoustic speed of Figure 1. The drift differences maximize at altitudes that are just below where relative drift starts to go down sharply, thereby indicating that the decrease in the magnitude of the relative drift $\mathbf{v}_d$ between ions and electrons is causing the decrease in the observed maximum phase velocity. The instability cone becomes narrower as v_d decreases, and the ion drift comes increasingly close to perpendicularity to $\mathbf{v}_d$, meaning that the ion drift contribution along the edge of the instability cone decreases even though the plasma is still unstable overall. It's just less unstable so that the ion drift contribution cannot be as large owing to geometric considerations.

The numbers displayed in the contour plots of Figures 3 and 4 also deserve a comment. First of all, the theory used to produce Figure 3 indicates that if the plasma density is large enough above 112 km to make the instability detectable, then the largest phase velocity observed from the ground over a wide field of view would go through a peak value between 114 and 118 km altitudes. Furthermore, that maximum would actually be rather close in both magnitude and direction to the $\mathbf{E} \times \mathbf{B}$ drift itself. Secondly, Figure 4 makes it very clear that once the altitude is above 105 km the ion drift can introduce phase velocities that quickly exceed the ion-acoustic speed by more than 200 m/s if the electric field is greater or equal to 75 mV/m in magnitude.

4.2 Fastest velocities predicted by the nonlinear Hysell model.

Hysell (2015, and references therein) assumed that the saturation speed decreased away from c_s with a $\cos\beta$ dependence away from the most unstable direction, which, in the generalized formulation, has to be taken as the $\mathbf{v}_d$ direction. St-Maurice and Chau (2016) added the ion drift contribution to this. In other words, their nonlinear expression for the phase velocity, v_{los}, along a line-of-sight was given by

$$v_{los} = \hat{\mathbf{k}}_p \cdot \mathbf{v}_d \frac{c_s}{v_d} + \hat{\mathbf{k}}_p \cdot \mathbf{v}_i \tag{14}$$

where $\hat{\mathbf{k}}_p = \mathbf{k}_p / k_p$ is just the direction of the primary unstable wave vector. With this in mind, we now generalize the Hysell ansatz by using $\mathbf{v}_d$ rather than $\mathbf{v}_e = \mathbf{E} \times \mathbf{b}/B$ as the reference direction since the most unstable modes are along $\mathbf{v}_d$ and not along $\mathbf{v}_e$.

It follows from Equation 14 that with the Hysell ansatz the nonlinear phase velocity is given by

$$v_{ph}^{NL} = c_s \cos\beta + v_i \sin\beta \tag{15}$$

where β is the angle between $\mathbf{k}_p$ and $\mathbf{v}_d$. As with the other isothermal model, at the edge of the unstable cone we must have the threshold velocity, meaning that at the maximum unstable angle of the cone, β_M, we must have $\cos\beta_M = v_d/c_s$. This means that depending on which side of $\mathbf{v}_d$ the $\mathbf{k}_p$ direction is, i.e., the wave vector selected by the radar line-of-sight direction is, we end up with

$$v_{ph}^{max} = c_s^* \left[\frac{c_s^*}{v_d} \pm \frac{v_i}{c_s^*} \sqrt{1 - \frac{c_s^{*2}}{v_d^2}} \right] \tag{16}$$

This final expression is identical to what we obtained for the other isothermal case (equation 13) except for the fact that the first term inside the square bracket is smaller, being now c_s^*/v_d instead of 1.

The next task is to compare the Hysell model results with those from the St-Maurice and Hamza model. The best way to assess the differences is though another figure that shows the result of the calculations for the same background model ionosphere. The 'Hysell model' results are shown in Figure 5. This figure shows that fast narrow velocity profiles extracted from the St-Maurice and Hamza versus Hysell models have significant differences. For one thing, with the 'Hysell model', the phase velocities keep increasing with altitude even by 120 km altitude instead of peaking near 116 km. The magnitudes in the

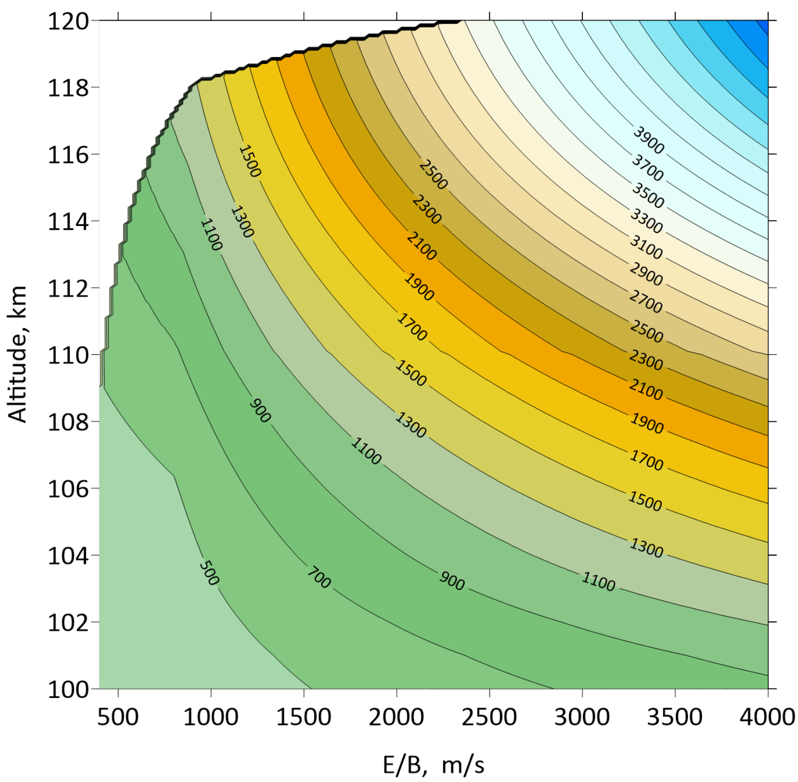

Figure 5. Same as for Figure 3 but for the 'Hysell isothermal model'.

Hysell model are also smaller than when we assume that saturation is at c_s irrespective of direction: adding a cosine dependence to the saturated phase velocity in the ion frame of reference makes the phase velocities smaller and narrows down the unstable cone, which in turn reduces the ion contribution.

4.3 Non-isothermal modifications to the ion drift contribution

Our presentation thus far has dealt with isothermal ions. However, Dimant and Oppenheim (2004) have pointed out that as the altitude approaches 120 km the ion heating is modulated in the waves themselves so that the description offered by the isothermal theory becomes less accurate. We are therefore now adding these effects to investigate where and if they become important for the computation of the maximum phase velocities.

While the present discussion is based on the Dimant and Oppenheim (2004) work, we follow here the formulation/notation used by St-Maurice and Chau (2016). The frequency is still given by Eqn 8. However, the growth rate is now given by

$$\gamma = \frac{\Psi}{1+\Psi}\frac{k_p^2 v_d^2}{\nu_i}\left[\frac{(1-1/\alpha_i^2)}{(1+\Psi)^2}\cos^2\beta + \frac{2}{3}\frac{(\cos\beta)/\alpha_i\,\{(\cos\beta)/\alpha_i - \sin\beta\}}{1+\Psi} - \frac{c_s^2}{v_d^2}\right] \tag{17}$$

where β is still the angle between $\mathbf{k}_p$ and $\mathbf{v}_d$. The growth rate depends on β because the Modulated Ion Ohmic Heating by Waves (MIOHW) inside the waves depends on the $\mathbf{k}_p$ direction. This means that T_i is enhanced with some wave vector directions and decreased for some other directions. This modulates the diffusion rate and introduces the complicated directional response shown by the equation. By contrast, in the isothermal case, the second term inside the curly brackets would not be present and the first term would not have the $(1-1/\alpha_i^2)$ factor in it.

We now use the same assumptions as for the isothermal calculations, namely, that the electric field inside the structures decreases through the introduction of a secondary wave vector $\mathbf{k}_s$ as the amplitude grows. This decrease continues until a zero growth rate is attained, at which point the structures reach their maximum amplitude. We chose once again to use $\Psi << 1$ since the altitude is high enough that unless there is a parallel component to the wave vector, this has to be the case. A second reason is that as long as Ψ is small (values of the parallel wavevector that are smalle enough), the threshold speed is smaller, making the instability cone wider and the contributions from the ion drift as large as can be on the edge of the instability cone.

In more precise terms, for a given direction β in waves that are strongly unstable, we assume from our nonlinear model that Equation 17 is set to zero through a decrease in the magnitude of the relative drift, v_d, just as was done for the isothermal case. This stated, the present focus of the paper is with fast narrow structures generated on the edge of the instability cone. In that case, we do not change v_d but we find instead for what value of β the growth rate approaches zero (marginally unstable modes). When v_d is large enough for a solution to $\gamma = 0$ from Equation 17 to exist (i.e. for a v_d/c_s ratio of order 1 or greater), there are in fact two solutions, one for $\sin\beta > 0$ and the other for $\sin\beta < 0$. In the first instance the ion drift adds to the Doppler shift, while in the second case, it reduces the drift (recall Figure 2). Note that the same situation existed in the isothermal case, with the difference for the isothermal case that the two solutions were identical aside from a change in the sign of $\sin\beta$. The non-isothermal case does not have this symmetry.

The zero growth rate calculation could be done analytically in terms of $x = \sin\beta$, but the calculations are cumbersome. We chose instead to build a simple solver that finds the two values of $\sin\beta$ for which $\gamma = 0$ in Eqn 17, assuming the v_d/c_s ratio is large enough for a real solution to exist. The values of $\sin\beta$ so obtained typically give the widths of the instability cone on each side of $\mathbf{v}_d$. Having found the angular spread on each side

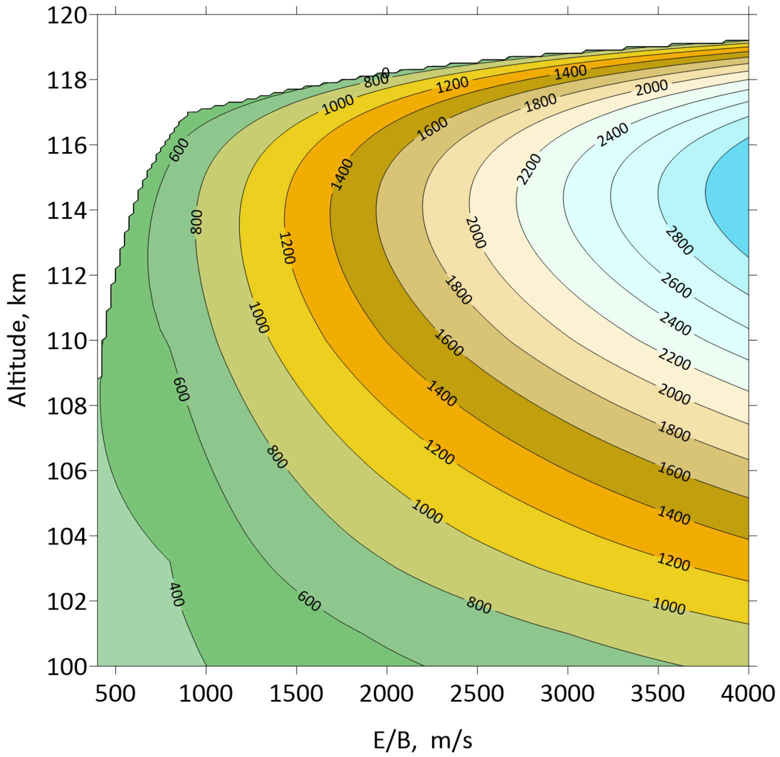

Figure 6. Same as Figure 3 but for the non-isothermal ion theory of the FB instability.

of the instability cone we can then add the ion drift contribution from $v_i \sin\beta$ as we did for the isothermal case, i.e. we add $v_{i0} \sin\beta = (v_d/\alpha_i)\sin\beta$ to c_s. For reference, note that in the isothermal case we would have found $v_d \cos\beta = c_s$, from which we would have stated that the marginally unstable waves were moving at c_s in the ion frame. The present procedure is similar.

A final remark is in order here: when α_i is of order 1 or less, and for weaker destabilizing values of v_d/c_s, there are some solution pairs for which $\sin\beta$ is negative in both instances. This means that even the fastest modes can actually move more slowly than c_s in such situations. This remains the exception as it only happens near the region for which the plasma is only marginally unstable overall, i.e., close to the top of the unstable layer.

The results of the non-isothermal calculations are shown in Figure 6 for the faster of the two solutions, namely, those for which $\sin\beta$ is positive. A first point to note is that below 115 km, the values obtained from the non-isothermal theory are rather similar to the isothermal case with the St-Maurice and Hamza model, though a bit smaller. Above 115 km, the net factor $[1-1/(3\alpha_i^2)]$ in front of the $\cos^2\beta$ term inside the square bracket on the RHS of Eqn 17 acts to decrease the growth rate. This happens because, by then, α_i becomes of order 1, which is reached at 118 km for our collision frequency model. A value of $\cos\beta$ closer to 1 is therefore required for instability so that the width of the unstable cone becomes smaller. As this happens, the contribution of the ion drift to the net Doppler shift has to decrease, since said contribution is from $v_i \sin\beta = (v_d/\alpha_i)\sin\beta$. A natural consequence is that, as seen in figure 6, the top boundary of the unstable region is lower than for the isothermal case.

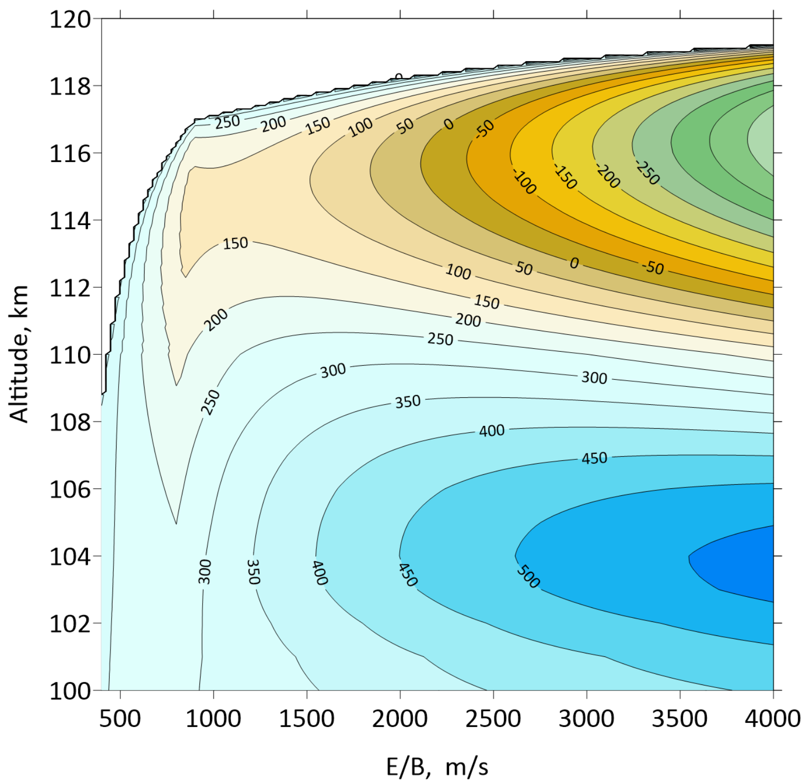

Figure 7. Same as Figure 6 but for the side of the instability cone where the ion drift reduces rather than increases the Doppler shift seen from the ground.

We conclude from Figure 6 that, like in the isotropic St-Maurice and Hamza model, the 'fast narrow' spectra (or Type IV as they have been labeled) keep getting faster with stronger electric fields. However, the peak values are smaller than predicted by the isothermal theory and the altitude of the peak Doppler shift is lower than for the isothermal case. At its peak, the maximum Doppler shift observable from the ground remains a few 100 m/s less than E/B, even though this is smaller than for the isothermal case with its somewhat higher altitudes and its maximum phase velocities approaching the value of E/B at the peak values.

4.4 Slow Doppler shifts with narrow spectral widths

While we have not until now covered the side of the unstable cone for which the ion drift reduces the Doppler shift observed from the ground, we do so here with Figure 7. The figure makes the point that the slow modes remain affected by the ion drift even around 105 km altitude and above. This creates a maximum in the slowest drifts around 104 km when the electric field is very strong ($E/B > 2000$ m/s). For weaker electric fields there is hardly any difference with the isothermal speed until we reach 110 km altitude. Above that height and for $E/B > 2000$ m/s, the slow Doppler shifts are more than 'slow' and they even take a sign opposite to that of the fast narrow modes. This is the result of having a decrease in c_s with altitude while v_i keeps increasing. When the electric field is very strong, the contribution from v_i is enhanced and this triggers a decrease in the threshold speed and therefore widen the negative side of the instabil-

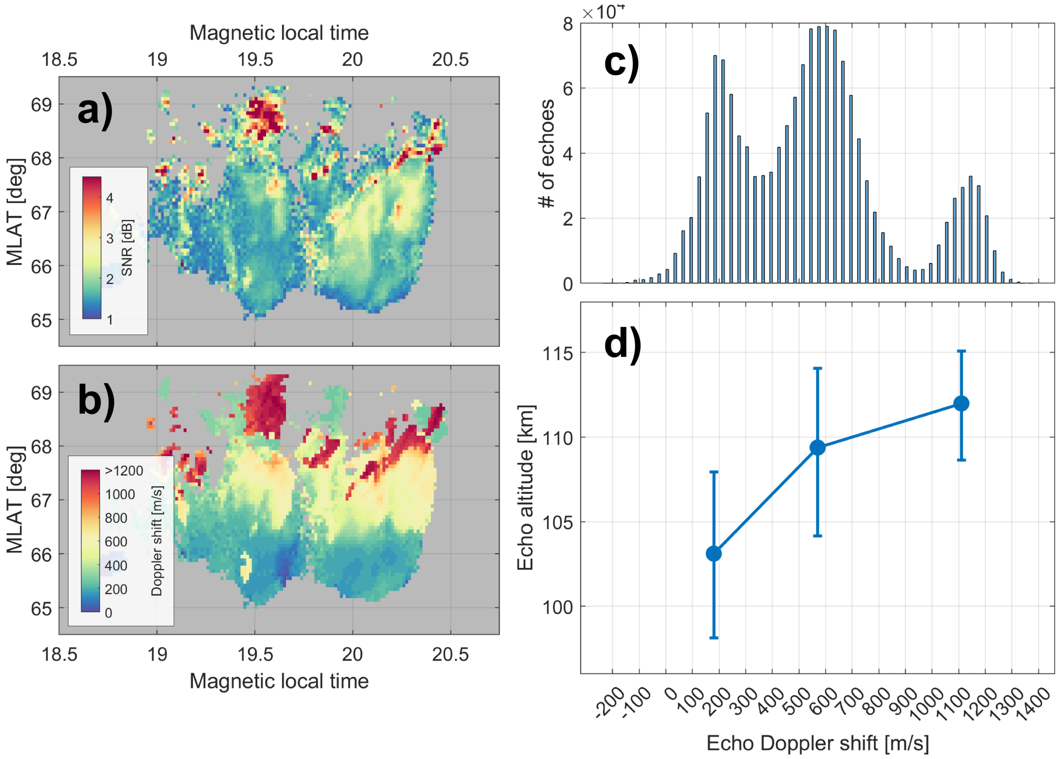

Figure 8. ICEBEAR 3D echoes observed during an active event on 25 April 2021. The leftmost panels (a and b) shows the signal-to-noise levels and various Doppler shifts observed as a function of MLT and Magnetic latitude between 02:30 UT and 04:30 UT. The rightmost panels (c and d) display the altitude distribution of echoes obtained in three successive Doppler shift speed bins 400 m/s wide, corresponding to the three populations evident in panel c). Panel d) shows the median and upper/lower quartile distributions of altitude in each Doppler bin. Note that we exclude the “west beam´´ of the ICEBEAR 3D data from the altitude calculations, where altitudes are anomalous.

ity cone. Similar outcomes for slow narrow spectra would have come from the isothermal theory.

5 Discussion

5.1 What model should we use?

While physical insights from the isothermal model prove to be useful, the non-isothermal results shown in Figures 6 and 7 are the ones we should pay attention to, because (1) non-isothermal effects simply cannot be ignored above 110 km and (2) we favor a model for which the direction for the limiting effects of diffusion on the growth rate is simply that of $\mathbf{k}_p$.

5.2 At what altitudes are fast Doppler shifts actually observed?

Figure 8 offers a preliminary view of some results obtained from the recently built ICEBEAR 3D coherent radar data (Lozinsky et al., 2022), which followed by a couple of years the advent of the already successful ICEBEAR radar (Huyghebaert et al., 2019;

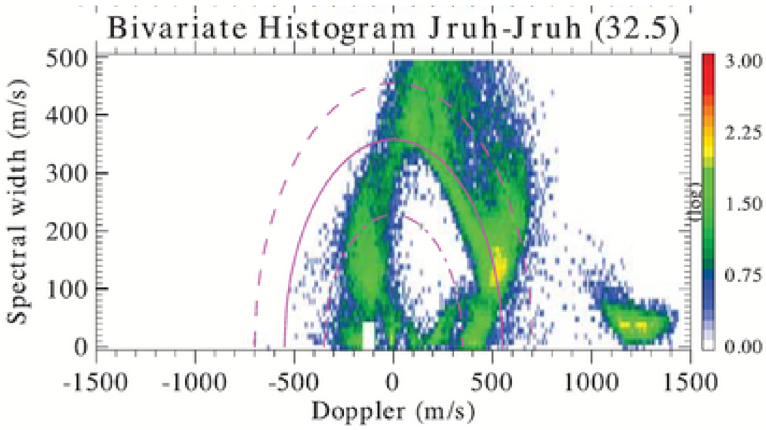

Figure 9. Bivariate histogram reproduced from part of Figure 6 in the Chau and St-Maurice (2016) paper. The data were acquired during a one hour interval during the peak of the major storm on March 17, 2015. The color scale refers to the log of the count.

Huyghebaert, McWilliams, et al., 2021). The echoes were extracted during a strong electric field event, when the IMF B_Z component was -5 nT on average and both the upper and lower envelope of the auroral electrojet index showed evidence for a considerable expansion of the auroral zone. The top and bottom left panels (a and b) on the left-hand-side show the signal-to-noise ratio and Doppler shift observed as functions of latitude and magnetic local time (same thing as if longitude had been swept). For the echoes in each of three wide Doppler speed bins, panel d) presents the median altitude position, with the error bars denoting upper and lower quartile distributions. While there are plenty of slower echoes at, say, 112 km, the figure illustrates that faster Doppler shifts only show up at higher altitudes. While there is at this point no clear determination of an altitude at which the Doppler shift might go through a maximum, we can nevertheless compare the information at hand against our preferred non-isothermal ion model. With a 1100 to 1200 m/s Doppler shift being observed on average between 110 and 115 km altitude Figure 6 indicates that E/B should be of the order of 1300 to 1500 m/s. This implies an electric field strength of the order of 65 to 75 mV/m.

5.3 First results on the observation of narrow spectra in light of the present theory

Figure 9 is a reproduction of one bivariate histogram which came as part of Figure 6 in Chau and St-Maurice (2016). The data were obtained during the afternoon of the particularly strong magnetic storm of March 17, 2015. The figure shows that a clear Type IV 'island' with very narrow spectral width was seen with a Doppler shift between 1200 and 1400 m/s. Interestingly, during strongly disturbed conditions, bi-variate histograms from the ICEBEAR datasets are very similar to the results posted by Chau and St-Maurice (2016). An example from the early days of ICEBEAR (*not* ICEBEAR 3D) is shown in Figure 10. We notet that, at the time, the ICEBEAR altitude could not be determined with great accuracy.

The narrow spectral lines at the bottom of the plots recorded in Figures 9 and 10 have to mean that the observed modes were only weakly unstable, i.e., $v_d \cos\beta$ was close to c_s. As discussed above, an additional contribution equal to $v_i \sin\beta$ would need to be added to this. Also, given the weakly growing conditions, we should have $\beta \to \beta_M$. Then, we have to recall that the only altitude where $\beta_M = 0$ has to be at the top of the unstable layer since, at that location, $\mathbf{v}_d$ is the only direction for which there is instabil-

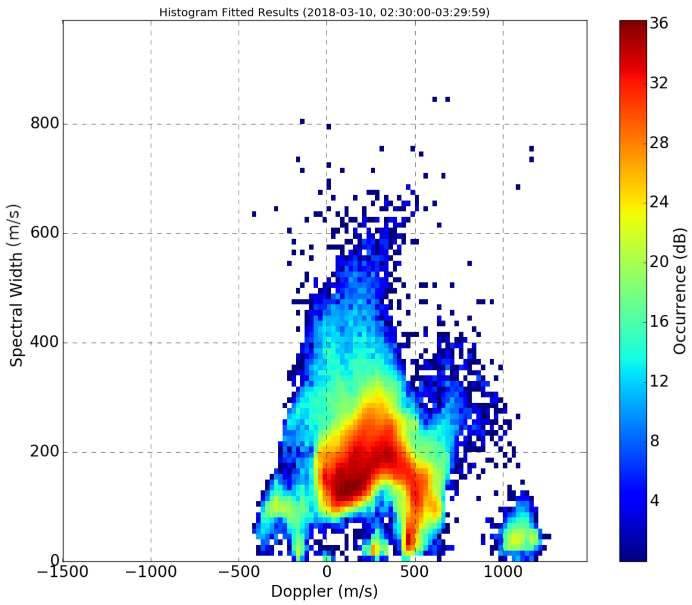

Figure 10. Same as in Figure 9 but for a disturbed period sampled by the ICEBEAR radar during its earlier days of operation. The spectra were measured on March 10, 2018, between 2:30 and 3:30 UT. Videos showing data with some overlap from this time period are provided in the Supplemental Material, highlighting the evolution and characteristics of the fast Doppler spectra measurements.

ity. By the same token, at any lower altitude in the unstable region, the $v_i \sin\beta_M$ term has to be added.

Figure 6 shows that there are many possible solutions to having narrow spectra with a 1300 m/s Doppler shift. For instance, at 103 km altitude, the calculations show that E/B should have been 4000 m/s. Noticing that for this condition c_s from Figure 1 would be around 850 m/s, this means that $v_i \sin\beta_M$ would have to account for 450 m/s. This is due, in this instance, to $v_i \sin\beta_M \approx v_i$ (very wide instability cone) and the fact that even with $\alpha_i \approx 10$ - as is the case around 103 km- we end up with a contribution from $v_i \sin\beta \approx v_i$ of the order of 400 m/s. Higher up, smaller values of E/B can accommodate the production of narrow spectra with 1300 m/s. Going all the way to top altitudes, the non-isothermal model indicates that there should be a very narrow transition to a 1300 m/s Doppler shift above 117 km, with a top altitude that does not change much with E/B.

The model calculations shown in Figure 6 indicate that the value of the observed Doppler shift from narrow spectra would maximize in the 112 to 116 km interval. This is the range of altitudes where, for a given value of E/B, the fastest narrow spectra would show up. Importantly, in addition, the approximate 5 km altitude interval would maximize the chances of detecting 'fast narrow' spectra. In that interval only some small variations in the Doppler shift would be expected. Specifically, a 1600 m/s E/B value would introduce Doppler shifts that vary by less than 50 m/s on each side of a 1300 m/s Doppler shift in the 111 to 116 km interval. Alternately, for the detection of 1200 to 1400 m/s Doppler shifts with narrow width spectra, we could infer that E/B should be between 1500 and 1750 m/s, according to Figure 6.

Another population of narrow spectral width echoes can also be seen in Figures 9 and 10, this time with a 350 to 450 m/s Doppler shift. There are no other narrow spectra between 450 m/s and 1100 m/s even though there are plenty of 'normal' Type I spectra with 150 to 350 m/s spectral widths and 500 to 700 m/s Doppler shifts (normal fully turbulent spectra associated with the most unstable directions that are little affected by the ion drift, as already discussed above). The Doppler shift of the slower narrow spectra fits very well with the lower peak that would take place between 102 and 107 km altitudes in Figure 7, which is predicted to be between 400 and 425 m/s for a 1500 to 1800 m/s E/B inferred from the Type IV (fast narrow) observations. In other words the bi-variate histograms are providing evidence for the fact that for modes near the 'edge of the instability cone' the ion drift does indeed create pairs of faster than c_s and slower than c_s echoes that differ from c_s by roughly the same amount. Unfortunately, the altitude information was not very reliable for the observations reported here, and the discussion must stop at that for now. However, we are inferring from the model calculations that the 400 to 500 m/s narrow echoes have to be coming from the lower part of the unstable region, around 104 km altitude. These echoes must therefore come from the edge of a strong 'Type I' echo region (type I echoes come from strongly unstable echoes with a c_s Doppler shift and are centered along the $\mathbf{v}_d$ direction). There is also a hint in the bi-variate histograms of a narrow population with Doppler shifts of the order of 100 to 200 m/s, which could be the high altitude complement to Type IV at 115 km altitude seen in Figure 7. It will be left to future studies with more accurate altitude and azimuthal determination to see if this notion is actually confirmed by the observations.

In light of the comparison between Figures 9 and 10, it is interesting to note that, in both cases, the bulk of the slower narrow Doppler shifts extends gradually towards the type I spectra as the spectral width increases. The pattern is basically a straight line in both examples. This could be explained by the fact that as the line-of-sight gradually deviates from the $\mathbf{v}_d$ direction in the bottom half of the unstable layer, the turbulence becomes gradually weaker (gradually narrower spectra) and the ion drift contribution gradually reduces the Doppler shift at the same time. To be specific, assume E/B to be what was associated with the fast narrow spectra, namely, 1500 to 1800 m/s. This means that the fully turbulent spectra from 102 to 107 km would have had a Doppler shift between 500 and 800 m/s, according to Figure 1. As already discussed above the weakly turbulent narrow spectra at those altitudes should have been of the order of 400 to 425 m/s.

The point is that a gradual rotation associated with azimuthal changes in the line-of-sight direction would have gradually taken the Doppler shift from $c_s \approx 700$ m/s at full turbulence to 425 m/s at weak turbulence. These numbers agree well with the 2-D histograms of Figures 9 and 10 . This being stated, we have to await an accurate determination of the altitudes of the various spectral types in order to confirm the theoretical interpretation.

The important point of the present subsection is that the narrow populations from the two separate events and different radars have very similar bi-variate histograms that indicate that strong electric field events create reproducible data that offer opportunities for promising future in-depth studies. This, incidentally includes the small population of narrow spectra with 100 m/s or so Doppler shifts. According to figure 3, this population could come from around 115 km altitude. However, it could also be associated with altitudes less than 100 km owing to non-isothermal electron effects lower down (St-Maurice & Chau, 2016), once again illustrating the importance of getting reliable altitude determinations for a clear understanding of the observations.

We conclude this subsection by pointing the reader to the Supplementary Information (SI) file linked to the present paper. The file points to two movies. The second one shows the location in latitude and longitude of the Doppler shifts that were observed around the time interval covered for the production of the bi-variate histogram of Figure 10 (the movie is from 3:00 TO 4:00 UT while the bi-variate histogram came from the 2:30 to 3:30 UT interval). The figure shows that the fast echoes came from a narrow pattern that was strongly elongated to the north, on the eastern edge of regions with smaller Doppler shifts. This orientation indicates that the $\mathbf{E}\times\mathbf{B}$ drift followed a rather long channel that was along a strongly northward direction. This facilitated the detection of fast echoes by the radar, given its field of view centered on the north.

The first movie from the SI file shows how the signal-to-noise ratio (SNR) changed in time as a function of Doppler shift and range. While the Doppler shift was recorded in Hz, we should note that the 400 Hz Doppler shifts came entirely from fast narrow spectra (or ‘Type IV’ spectra). The movie illustrates that the Type IV signatures were connected to regions for which the Doppler shifts of other modes were also in excess of 700 m/s but were detached from them. We take this as an indication that with its azimuthal fan, the radar was able to detect the fastest modes (more or less in the $\mathbf{E}\times\mathbf{B}$ direction) at the same time as it was detecting normal ‘Type I’ signatures associated with full turbulence in the $\mathbf{v}_d$ rather than in the $\mathbf{E}\times\mathbf{B}$ direction. The cause for the gap between the two signatures is not entirely clear. One possibility is that the signal-to-noise measured the ratio of the peak spectral value to the background noise. For strong turbulence this is not an issue. However, for very narrow spectral widths associated with weak turbulence the signal will stand out more even if the integrated signal is less, thereby enhancing the chances for the detection of spectra with the narrowest spectral widths. The only thing we can tell for sure at this point is that the fully turbulent spectra and the fast weakly turbulent spectra would have come from different lines-of-sight. Clearly, this points to far more detailed future studies in relation to locations of echo types from high resolution data in time and space.

5.4 Points to keep in mind for future higher resolution studies

The following points should be kept in mind when studying the occurrence of narrow spectral signatures:

1. The generation of bi-variate histograms of the type presented in the previous subsection requires that the plasma density at the altitudes of interest be high enough. In practise, not all unstable structures should be visible for coherent radars. The cross section dependence on $\delta n_{\mathbf{k}p}$ makes the intensity of the signal proportional to $|\frac{\delta n_{\mathbf{k}p}}{n_0}|^2 n_0^2$. The density fluctuation levels vary a lot less than n_0^2 in the presence of the details of precipitation (typical auroral situations). Therefore, whether or not a large amplitude structure is seen could well depend on precipitation details. Evidence for this effect has been reported recently by Huyghebaert, St. Maurice, et al. (2021) through the use of combined coherent radar and optical observations from the Swarm-E satellite. Basically, the authors found that FB irregularities were not detected when the plasma density was too high owing to a probable shorting of the electric field. They were also not detected when the plasma density was low, presumably because the radar cross-section was too small. Future ground-based optical observations or satellite precipitation observations in combination with simultaneous coherent radar observations are needed to ascertain how important the plasma density effects might be.
2. The data presented in this paper are preliminary in the sense that no attempt has been made to extract precise information about the distribution of Doppler shifts through the field of view of the instrument. All we showed in the present preliminary presentation is (1) that faster Doppler shifts have to come from the higher part of the unstable region; (2) that there will be a population of narrow spectra coming from higher altitudes that will have Doppler shifts well in excess of c_s, while spectra with a somewhat lower Doppler shift than c_s would come from the lower part of the unstable region. Narrow spectra with a Doppler shift much lower than c_s spectra should be present at the same altitude as the fast narrow spectra. This suggests, (3), that it might be feasible to use our model calculations to infer useful information about the electric field responsible for the generation of unstable FB waves after an accurate determination of the location of the various spectra with narrow spectral widths becomes available.
3. The model calculations should be viewed as providing an upper limit on the Doppler shift of fast narrow spectra. We should expect a collection of Doppler shifts that are close to what we have calculated but do not exceed that upper limit. Together with small Doppler shift variations over 'wide ranges' (5 km) of altitude the existence of a small non-zero range of values for narrow spectra may be the reason why the Type IV 'islands' have somewhat variable Doppler shifts and spectral widths. It might also explain, as we discussed, the 'straight line' population that extends from 500 to 750 m/s Doppler shifts as the spectral width increases from 30 to 300 m/s.
4. It should be kept in mind that the slower branch of the narrow spectra occurs on one side of the instability cone while the fast branch comes from the other side of it. This means that even if the electric field were to be very uniform throughout the field of view of a radar, the two types of narrow spectral echoes should come from different directions possibly tens of degrees apart in azimuth.
5. When the central viewing direction is to the north as is the case with ICEBEAR, we should expect to see narrow spectral signatures around magnetic midnight because the $\mathbf{E}\times\mathbf{B}$ drift would have a better chance to be moving towards the radar, making it easier to detect the various spectral signatures of interest. This being stated, an active auroral event is full of twists and turns so that a northward looking radar could still be yielding narrow spectral results in the dusk or dawn sectors. The SI file added to the present paper provides an example of this very situation.
6. Equatorial observations of FB waves have clearly demonstrated that gradient-drift waves a few km in size are capable to rotate the electric field direction in FB structures (Kudeki et al., 1982) with an oscillating pattern matching the oscillation of the gradient-drift wave. As a result, for a radar facing magnetic north, one would

expect to often face an east-west electric field with gradient-drift structures producing oscillating $\mathbf{E}\times\mathbf{B}$ drifts on a scale of a few km in the electric field direction. Given the successful equatorial observations, it might be feasible to detect such oscillating structures either with a high time resolution observation at a fixed location or, better still, with a high-azimuthal resolution combined with a high time resolution.

6 Summary and Conclusion

We have shown that the phase velocity of FB waves reaches a maximum between 114 and 118 km, but only in the case of spectra with narrow spectral widths. The reason is that the background ion drift can affect the Doppler shift of weakly turbulent modes, but not the Doppler shift of fully turbulent modes, owing to a peculiarity of the geometry having to do with the ion drift being perpendicular to the relative drift between electrons and ions.

Following a comparison between weakly turbulent isothermal and non-isothermal ion calculations, we have also found that non-isothermal ion corrections to the weakly unstable theory become important because the fastest modes occur in a region where non-isothermal ions affect the dispersion relation. The calculations reveal that, by comparison to the isothermal situation, the non-isothermal ion corrections create fastest phase velocities that are smaller than for the isothermal case by a few 100 m/s when the electric field is very strong (75 mV/m and more). In fact, isothermal theory would have predicted that the maximum phase velocity of spectra with narrow spectral widths would otherwise have been very close to the $\mathbf{E}\times\mathbf{B}$ drift. Both theories predict that the fastest waves should be seen if the look direction matches the $\mathbf{E}\times\mathbf{B}$ direction itself, this in spite of smaller growth rates along that direction. This condition requires the ion drift to be large enough to bring the observed phase velocities back from a c_s value toward the largest possible values that can be achieved by the plasma waves, namely, the value of the mean electron drift, i.e., the $\mathbf{E}\times\mathbf{B}$ itself.

We noted that at the upper altitudes of the unstable region the ion drift can also trigger narrow slow modes when the look direction shifts toward the electric field direction. As a result, narrow spectra from the upper part of the unstable region end up not just with a total Doppler shift that can be substantially greater than c_s, but also with another narrow spectral mode that can be substantially smaller than c_s. This being stated, the bulk of the 'slow narrow' spectra with Doppler velocities only moderately less than c_s by 100 to 200 m/s would be found lower down, near 105 km altitude. We also recalled that St-Maurice and Chau (2016) showed that other slow narrow spectral populations should be present below 100 km owing to a non-isothermal electron behavior there. This point illustrates the importance of a reliable altitude determination if we are to understand the observations before we can exploit their contents.

We should note the large ion drifts have to also impact the Doppler shift of secondary waves (so-called Type II waves) so that secondary waves with very large spectral width (expected when the ion-acoustic speed is large, according to Hamza and St-Maurice (1993)) will start to move at measurable speeds, namely the ion drift component along the electric field direction, when created in the upper part of the unstable region during strong electric field conditions.

Future research should be aimed at producing as detailed a description as possible of the spectral width and the altitude and azimuthal position of the various kinds of echoes. It could ultimately be used to document how the electric field changes within the field of view, at least when strong electric fields are present. It might even enable the detection of a modulation by larger size gradient-drift waves, much as has been seen in equatorial situations.

Acknowledgments

This work was supported by discovery grants from the Natural Science and Engineering Research Council (NSERC) of Canada [RGPIN-04891-2017 for JPSM and RGPIN-19135-2019 for GCH], the Solar-Terrestrial Science Data Analyses program from the Canadian Space Agency (CSA) [21SUSTIER] , and the Norwegian Research Council. Support for the data studies was also received from from the Digital Research Alliance of Canada [RRG-FT2109]. For ICEBEAR data per se, we acknowledge the support of the CSA [20SUGOICEB], the Canada Foundation for Innovation (CFI) John R. Evans Leaders Fund [32117] and the Province of Saskatchewan. We also acknowledge the important contribution of the entire ICEBEAR engineering team (notably, Draven Galeschuk, Brian Pitzel and Adam Lozinsky) at the University of Saskatchewan, without whom ICEBEAR data would simply not exist. The ICEBEAR data are available from Icebear.usask.ca.

References

Chau, J. L., & St-Maurice, J.-P. (2016). Unusual E region echoes observed at mid-latitudes during the March 17, 2015 storm with the use of multi-static, multi-frequency VHF radar links. *Journal of Geophysical Research: Space Physics*, *xxx*(x), submitted. (Publisher: Wiley Online Library)

Dimant, Y. S., & Oppenheim, M. (2004). Ion thermal effects on E-region instabilities: linear theory. *Journal of atmospheric and solar-terrestrial physics*, *66*(17), 1639–1654. (Publisher: Elsevier)

Drexler, J., St-Maurice, J.-P., Chen, D., & Moorcroft, D. (2002). New insights from a nonlocal generalization of the Farley-Buneman instability problem at high latitudes. *Annales Geophysicae*, *20*(12), 2003–2025.

Fejer, B. G., Farley, D. T., Balsley, B. B., & Woodman, R. F. (1975). Vertical Structure of the VHF Backscattering Region in the Equatorial Electrojet and the Gradient Drift Instability. *J. Geophys. Res.*, *80*(10), 1313–1324. (Place: Balsley's)

Fejer, B. G., & Kelley, M. (1980). Ionospheric irregularities. *Reviews of Geophysics*, *18*(2), 401–454. (Publisher: Wiley Online Library)

Hamza, A. M., & St-Maurice, J. P. (1993). A self-consistent fully turbulent theory of auroral E region irregularities. *Journal of Geophysical Research: Space Physics*, *98*(A7), 11601–11613. Retrieved from `http://dx.doi.org/10.1029/92JA02835` doi: 10.1029/92JA02835

Huyghebaert, D., Hussey, G., Vierinen, J., McWilliams, K., & St-Maurice, J.-P. (2019). ICEBEAR: An all-digital bistatic coded continuous-wave radar for studies of the E region of the ionosphere. *Radio Science*, *54*(4), 349–364. (Publisher: AGU)

Huyghebaert, D., McWilliams, K., Hussey, G., Galeschuk, D., Chau, J. L., & Vierinen, J. (2021). Determination of the azimuthal extent of coherent E-region scatter using the ICEBEAR linear receiver array. *Radio Science*, *56*(3), 1–18. (Publisher: AGU)

Huyghebaert, D., St. Maurice, J.-P., McWilliams, K., Hussey, G., Howarth, A. D., Rutledge, P., & Erion, S. (2021). The Properties of ICEBEAR E-Region Coherent Radar Echoes in the Presence of Near Infrared Auroral Emissions, as Measured by the Swarm-E Fast Auroral Imager. *Journal of Geophysical Research: Space Physics*, *126*(12), e2021JA029857. (Publisher: Wiley Online Library)

Hysell, D. L. (2015). The radar aurora. *Auroral dynamics and space weather*, *215*, 193. (Publisher: John Wiley & Sons, Inc Hoboken, NJ)

Kelley, M. C. (1989). *The Earth's Ionosphere: Plasma Physics and Electrodynamics.* Academic, San Diego, Calif.

Kudeki, E., Farley, D. T., & Fejer, B. G. (1982). Long Wavelength Irregularities in the Equatorial Electrojet. *Geophys. Res. Lett.*, *9*, 684.

Lozinsky, A., Hussey, G., McWilliams, K., Huyghebaert, D., & Galeschuk, D. (2022). ICEBEAR-3D: A Low Elevation Imaging Radar Using a Non-Uniform Coplanar Receiver Array for E Region Observations. *Radio Science*, *57*(3), e2021RS007358. (Publisher: Wiley Online Library)

Oppenheim, M., & Dimant, Y. S. (2013). Kinetic simulations of 3-D Farley-Buneman turbulence and anomalous electron heating. *Journal of Geophysical Research: Space Physics*, *118*(3), 1306–1318. (Publisher: Wiley Online Library)

Prikryl, P., Andre, D., Koehler, J., Sofko, G., & McKibben, M. (1990). Evidence of highly localized auroral scatterers from 50-MHz CW radar interferometry. *Planetary and Space Science*, *38*(7), 933–944. (Publisher: Elsevier)

Prikryl, P., Andre, D., Sofko, G., & Koehler, J. (1988). Doppler radar observations of harmonics of electrostatic ion cyclotron waves in the auroral ionosphere. *Journal of Geophysical Research: Space Physics*, *93*(A7), 7409–7424. (Publisher: Wiley Online Library)

Sahr, J. D., & Fejer, B. G. (1996). Auroral electrojet plasma irregularity theory and experiment: A critical review of present understanding and future directions. *Journal of Geophysical Research: Space Physics*, *101*(A12), 26893–26909. Retrieved from `http://dx.doi.org/10.1029/96JA02404` doi: 10.1029/96JA02404

Sangalli, L., Knudsen, D., Larsen, M. F., Zhan, T., Pfaff, R., & Rowland, D. (2009). Rocket-based measurements of ion velocity, neutral wind, and electric field in the collisional transition region of the auroral ionosphere. *Journal of Geophysical Research: Space Physics*, *114*(A4). (Publisher: Wiley Online Library)

Sato, T. (1973). Unified theory of type I and II irregularities in the equatorial electrojet. *Journal of Geophysical Research*, *78*(13), 2232–2243. (Publisher: Wiley Online Library)

Schunk, R., & Nagy, A. (2009). *Ionospheres: physics, plasma physics, and chemistry.* Cambridge university press.

St-Maurice, J.-P., & Chau, J. L. (2016). A theoretical framework for the changing spectral properties of meter-scale Farley-Buneman waves between 90 and 125 km altitudes. *Journal of Geophysical Research: Space Physics*, *121*(10). (Publisher: Wiley Online Library)

St-Maurice, J.-P., Cussenot, C., & Kofman, W. (1999). On the usefulness of E region electron temperatures and lower F region ion temperatures for the extraction of thermospheric parameters: a case study. *Annales Geophysicae*, *17*(9), 1182–1198.

St-Maurice, J.-P., & Goodwin, L. (2021). Revisiting the Behavior of the E-Region Electron Temperature During Strong Electric Field Events at High Latitudes. *Journal of Geophysical Research: Space Physics*, *126*(2), 2020JA028288. (Publisher: Wiley Online Library)

St-Maurice, J.-P., & Hamza, A. (2001). A new nonlinear approach to the theory of E region irregularities. *Journal of Geophysical Research: Space Physics*, *106*(A2), 1751–1759. (Publisher: Wiley Online Library)

St. Maurice, J.-P., & Schlegel, K. (1983). A theory of coherent radar spectra in the auroral E region. *Journal of Geophysical Research: Space Physics*, *88*(A5), 4087–4095. (Publisher: Wiley Online Library)

Supporting Information for the paper "Narrow width Farley-Buneman spectra under strong electric field conditions"

Jean-Pierre St-Maurice[13], Devin Huyghebaert[4], Magnus F. Ivarsen[12], , and

Glenn C. Hussey[1]

[1]Department of Physics and Engineering Physics, University of Saskatchewan, Saskatoon, Saskatchewan, Canada

[2]Department of Physics, University of Oslo, Oslo, Norway

[3]Department of Physics and Astronomy, University of Western Ontario, London, Ontario, Canada

[4]Department of Physics and Technology, UiT The Arctic University of Norway, Norway

Contents of this file

Additional Supporting Information (Files uploaded separately)

1. Captions for Movies S1 and S2

Introduction

The present material provides the reader with context for the measurements presented in the main article. The first video (Movie S1) displays data obtained from the Ionospheric Continuous-wave E-region Bistatic Experimental Auroral Radar (ICEBEAR) plotted in a range-Doppler grid with the color representing the Signal-to-Noise-Raio (SNR). The time resolution of the measurements is 5 seconds. There are multiple instances of relatively fast Doppler velocity spectra, where a theoretical interpretation for the occurrence of these

---

fast narrow spectra is provided in the manuscript. In the second video (movie S2), the data is mapped to the ICEBEAR field-of-view using azimuthal and range information.

Movie S1. Movie showing the range and Doppler shift evolution of ICEBEAR spectra with a 5 s time resolution. The movie was recorded over the time period 3:00-4:00 UT on March 10, 2018. To convert the Doppler shift to an approximate velocity one can multiply by 3.03 m (half-wavelength of the ICEBEAR 49.5 MHz radar operating frequency).

Movie S2. Movie showing the evolution of ICEBEAR measurements mapped to the radar field-of-view with a time resolution of 5 seconds over the time period of 3:00-4:00 UT on March 10, 2018. The azimuthal information from the linear ICEBEAR interferometer (pre-ICEBEAR 3D) were used to map the coherent scatter.